IEEE Access
Multidisciplinary | Rapid Review | Open Access Journal

Received November 7, 2019, accepted December 1, 2019, date of publication December 9, 2019,
date of current version December 23, 2019.

Digital Object Identifier 10.1109/ACCESS.2019.2958347

Energy-Efficient Full-Duplex Concurrent Scheduling Based on Contention Graph in mmWave Backhaul Networks

JING LI[1,2], YONG NIU[1,2], (Member, IEEE), HAO WU[1,2], (Member, IEEE), BO AI[1,2], (Senior Member, IEEE), ZHANGDUI ZHONG[1,2], (Senior Member, IEEE), AND SHIWEN MAO[3], (Fellow, IEEE)

[1]State Key Laboratory of Rail Traffic Control and Safety, Beijing Jiaotong University, Beijing 100044, China
[2]Beijing Engineering Research Center of High-speed Railway Broadband Mobile Communications, Beijing Jiaotong University, Beijing 100044, China
[3]Electrical and Computer Engineering Department, Auburn University, Auburn, AL 36849-5201, USA

Corresponding author: Yong Niu (niuy11@163.com)

This study was supported by National Key R&D Program of China under Grant 2016YFE0200900; and by the National Natural Science Foundation of China Grants 61725101, 61801016, and U1834210; and by the China Postdoctoral Science Foundation under Grant 2018T110041; and by the Beijing Natural Fund under Grant L172020; and by Major projects of Beijing Municipal Science and Technology Commission under Grant No. Z181100003218010; and by the NSF under Grant ECCS-1923717; in part by the State Key Lab of Rail Traffic Control and Safety, Beijing Jiaotong University, under Grants RCS2019ZZ005 and RCS2019ZT006; in part by the funding under Grant 2017RC031.

ABSTRACT In the fifth generation (5G) era, dense deployment of small cells and full-duplex (FD) technology applications are two key features of millimeter-wave (mmWave) wireless communication systems, which offer the opportunity to meet the explosive growth of data service requirements. It is the beamforming and advances in analog as well as digital self-interference (SI) cancellation schemes that improve the network capacity in mmWave wireless backhaul networks. To achieve power saving and further network performance optimization, we propose a FD concurrent transmission mechanism employed in a mmWave backhaul network. Contention graph is constructed in consideration of multi-user interference (MUI), SI, and FD transmission constraints. Then flow-grouping and power control algorithms are proposed based on the contention graph. We evaluate the performance of the proposed algorithm in terms of energy consumption, achievable network throughput, and energy efficiency. The impact of the interference threshold on the system performance is also investigated when the distribution of base stations (BSs), traffic loads, and maximum transmission powers change. Simulation results illustrate that with proper SI cancellation and interference threshold, the proposed concurrent mechanism outperforms time-division multiple access (TDMA), half-duplex (HD) concurrent transmission, and FD concurrent transmission without power control.

INDEX TERMS Millimeter-wave, wireless backhaul networks, contention graph, full-duplex, concurrent transmission.

I. INTRODUCTION

To meet the explosive growth of data rate and bandwidth requirements in new technologies such as Industrial Internet of Things (IIoT), Artificial Intelligence (AI) and big data analytics, millimeter-wave (mmWave) communications have been proposed to be one of the key technologies in the fifth generation (5G) cellular networks. The advantages of the mmWave band not only include the availability of gigahertz underutilized spectrum, but also the line of sight (LOS) characteristic of communication, which contributes to interference control [1]. However, due to the dense deployment of base stations (BSs) in mmWave backhaul networks, it is a considerable expense to use traditional optic fiber networks between BSs [2]. In contrast, wireless backhaul networks using beamforming and directional antennas have significant advantages in terms of throughput and deployment costs [3], [4]. The deployment of directional antennas can effectively resist the attenuation of mmWave transmission in wireless backhaul networks, whereas the beamforming technology helps to increase the throughput and extend the propagation range.

The associate editor coordinating the review of this manuscript and approving it for publication was Lin Bai.

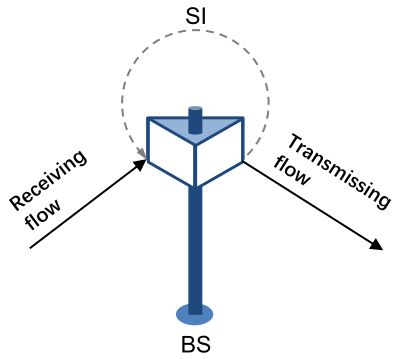

FIGURE 1. Illustration of the SI caused by full-duplex transmissions.

In the past decade, considerable studies have been made on the energy efficiency of wireless backhaul networks, including a comparison study of network architectures and frequency bands in [5]. It is shown that concurrent transmissions of data flows provide higher network throughput, but the energy consumption maintains at a high level, which is tightly related to the severe interference in parallel transmission. Multiple investigations have been made on this issue in [6]–[11], where concrete progress has been made in both medium access control (MAC) protocol design, frame scheduling, and interference cancellation. For example, the authors in [9] proposed an adaptive channel-superframe allocation algorithm based on a newly designed superframe structure, which achieved superiority in quality of service (QoS). Reference [11] proposed a novel link scheduling strategy for concurrent transmissions based on the feedback beamforming information in mmWave networks. However, most exiting scheduling algorithms in mmWave bands can only work at the half-duplex (HD) mode, which limits spectral efficiency so that cannot deliver increasing data rate [12]. Compared with HD mode, full-duplex (FD) as the method to transmit and receive data flow simultaneously, nearly doubles the system capacity, which is very impressive for mmWave communication system. Moreover, FD mode shows superiority in bit error rate reduction and outage probability control, which offering the potential to the evolution of state-of-the-art technologies in 5G [12]. However, the problem of self-interference (SI), as shown in Fig. 1, occurs in FD systems. The SI is caused by the transmitted signal to the received signal at the same BS when the same channel is used for receiving and transmission [13]. Although several of novel economic designs for SI cancellation have been proposed in [14]–[18], there is still remaining self-interference (RSI) which has a negative impact on the concurrent transmission and system performance. Thus, to improve energy efficiency, the design of concurrent scheduling in FD mode should take SI into consideration.

Furthermore, military, industry, and academia all show great interests in mmWave communication technologies, while significant progress has been made in beamforming design, channel estimation, signal detection, multiple access scheme application, and capacity evaluation [19]–[26]. As the first step to set up communications in burst mmWave wireless systems, robust package detection mechanism is of importance. Also, mmWave antennas with wide bandwidth and good directional radiation patterns have been proposed [27]. Besides, Zhu *et al.* in [25] investigated the application of non-orthogonal multiple access (NOMA) in mmWave communication, aiming to increase the total number of served users. The fact is that communications at such high frequencies not only require the application of robust signal detection mechanism as well as suitable multiple access scheme and the deployment of enhanced directional antennas, but also represent a paradigm-shift for network control and resource management. The performance evaluation of backhaul wireless networks should focus on energy consumption as well as network throughput. With these motivations, we propose an energy efficient concurrent scheduling algorithm in FD mmWave backhaul networks, aiming to achieve a superior performance in both energy consumption and network throughput. The main contributions of this paper are summarized as follows.

- We introduce FD into concurrent transmission scheduling in a mmWave backhaul network. Combining the transmission features of traditional time-division multiple access (TDMA) and FD modes in mmWave bands, we establish a joint optimization model to enhance the energy efficiency of the system.
- Fully considering the principle of parallel transmission and FD advantages as well as practical constraints, we propose a concurrent scheduling algorithm which includes a flow-grouping algorithm and a power control algorithm, where the former is constructed based on an established contention graph, which effectively reduces the serious interference, and the latter devotes to reducing unnecessary energy consumption as well as enhancing network throughput.
- We evaluate the impact on energy consumption, network throughput, and energy efficiency of various scheduling schemes, traffic loads, and flow numbers. We also analyze how to properly set the interference threshold σ, when the traffic loads, the distribution of BSs, and the maximum transmission power vary.

The rest of this paper is organized as follows. In the next section, the superframe structure, antenna model, and different transmission modes are described. In Section III, the joint optimization problem in FD mmWave backhaul networks is formulated. In Section IV, the proposed flow-grouping algorithm and the power control algorithm are presented. In Section V, the simulation study is presented. Finally, conclusions are given in Section VI.

II. PRELIMINARIES AND TRANSMISSION MODES

A. SUPERFRAME STRUCTURE

As stated in [28], [29], frame-based scheduling directional MAC (FDMAC) leverages collision-free concurrent

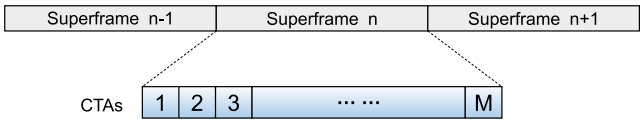

FIGURE 2. The frame structure of mmWave communications.

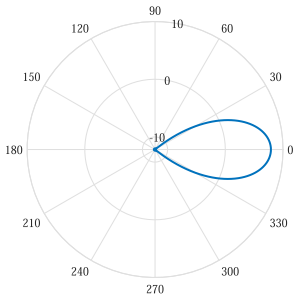

FIGURE 3. The pattern of the directional antenna deployed in mmWave communications.

transmissions to fully exploit spatial reuse in mmWave communications, with which network time is partitioned into a sequence of non-overlapping intervals. These intervals are defined as superframes (SFs) in IEEE 802.15.3 [30]. In our proposed system, each SF is further partitioned into M time slots called channel time allocations (CTAs). A typical SF structure is illustrated in Fig. 2.

B. ANTENNA MODEL

According to IEEE 802.15, taking both beamforming information and spatial reuse conditions into consideration, the most widely used realistic directional antenna model in mmWave-band networks [31], as illustrated in Fig. 3, is adopted in this paper, which can be described as

$$G(\theta) = \begin{cases} G_0 - 3.01\cdot(\frac{2\theta}{\theta_{-3dB}})^2, & 0^\circ \le \theta \le \theta_{ml}/2 \\ G_{sl}, & \theta_{ml}/2 \le \theta \le 180^\circ, \end{cases} \quad (1)$$

where θ is the receiving angle with the value in $[0^\circ, 180^\circ]$. θ_{-3dB} represents the angle of the half-power beamwidth, and $\theta_{ml}/2$ is the main lobe width of the antenna model, which is equal to $2.6\cdot\theta_{-3dB}$. G_0 is the maximum antenna gain while G_{sl} is the side lobe gain, which can be denoted by

$$G_0 = 10\log(1.6162/\sin(\theta_{-3dB}))^2, \quad (2)$$

$$G_{sl} = -0.4111 \cdot \ln(\theta_{-3dB}) - 10.579. \quad (3)$$

C. TRANSMISSION MODES

In this section, we compare several fundamental capacities under three transmission modes, i.e., TDMA mode, HD mode, and FD mode. TDMA adopts a sequential transmission scheme while the other two make full use of concurrent transmissions. Without loss of generality, we assume that flow transmission between densely deployed BSs in the mmWave backhaul network satisfies the LOS condition.

1) TDMA MODE

According to the path loss model in [32], the received power of flow i at BS r_i from the transmission BS t_i can be denoted by

$$P_r(t_i, r_i) = kP_tG_t(t_i, r_i)G_r(t_i, r_i)D_{t_ir_i}^{-n}, \quad (4)$$

where k is a constant proportional to $(\lambda/4\pi)^2$, in which λ represents the wavelength. P_t is the transmission power of flow i, and n is the path loss exponent related to the propagation environment. For flow i, $G_t(t_i, r_i)$ and $G_r(t_i, r_i)$ denote the antenna gain at the transmitter and receiver respectively in the direction of t_i to r_i, and $D_{t_ir_i}$ is the distance between t_i and r_i. By Shannon's theorem, the data rate of flow i in the TDMA mode can be calculated by

$$R_i = \eta W\log_2\left(1 + \frac{P_r(t_i, r_i)}{N_0W}\right), \quad (5)$$

where $\eta \in (0,1)$, W denotes the bandwidth, and N_0 is the one-side noise power spectral density of Gaussian noise [33]. Thus, the throughput of flow i can be calculated by

$$Q_i = \frac{R_i \cdot \xi_i}{M}, \quad (6)$$

in which ξ_i is the number of CTAs needed by the transmission of flow i, and M is the total number of CTAs in one SF.

2) CONCURRENT TRANSMISSION

Unlike TDMA, concurrent transmissions first divide flows into several groups according to constraints of transmission modes. Then the number of CTAs in each group will be re-allocated, and flows scheduled in the same group can share the re-allocated θ CTAs during transmission. Generally, $\theta \ge \xi_i$, so that with the same network throughput requirement as TDMA, the transmission rate and transmission power of each flow can be reduced.

a: HALF-DUPLEX MODE

The HD transmission mode, which is adopted in most of the current wireless communication systems, transmits and receives signals in two orthogonal channels, respectively. To achieve concurrent transmissions, the conflicts and interference among flows should be considered. Due to the HD mode, any two flows sharing a common BS cannot be transmitted concurrently. Also, the multi-user interference (MUI) between flows should be taken care of. When parallel transmissions are adopted, the received interference at r_i from t_j can be expressed as

$$P_r(t_j, r_i) = \rho kP_tG_t(t_j, r_i)G_r(t_j, r_i)D_{t_jr_i}^{-n}, \quad (7)$$

where ρ denotes the MUI factor related to the cross correlation of signals from different links [33]. Assume that flows are divided into K_1 groups in HD mode, and then in the k_1th group with ν flows scheduled, the data rate achieved by flow i can be denoted by

$$R_i^{hd} = \eta W\log_2\left(1 + \frac{P_r(t_i, r_i)}{N_0W + \sum_{\nu} a_i^{\nu}P_r(t_j, r_i)}\right), \quad (8)$$

where for each flow j ($j \neq i$) scheduled in the k_1th group, a_i^v is a binary variable which denotes whether MUI exists in flow j and flow i. If so, $a_i^v = 1$; otherwise, $a_i^v = 0$. Thus, $\left(\sum_v a_i^v P_r(t_j, r_i)\right)$ is the total MUI received by flow i. And the throughput of flow i can be calculated by

$$Q_i^{hd} = \frac{R_i^{hd} \cdot \theta^{k_1}}{M}. \tag{9}$$

b: FULL-DUPLEX MODE

As shown in Fig. 4, unlike the BS used in HD strategies, the BS deployed in a FD system should be equipped with both a transmitting antenna and a receiving antenna, which enable simultaneous transmission and reception of downlink and uplink traffic in the same frequency band [34]. Similar to HD mode, flow scheduling in FD mode should also consider conflicts and interference among flows, which is more complicated and is illustrated in detail in part A of Section IV. The point is that we are explaining the FD mode under the situation that significant progress has been made in SI cancellation. Nowadays, typical FD systems deploy both passive suppression like directional isolation, absorptive shielding, etc. and active cancellation techniques including digital SI cancellation, which together realize more than 110 dB SI cancellation [35]–[37]. Here, we assume that flows are divided into K_2 groups in FD mode, and then in the k_2th group with μ flows transmitted concurrently, the data rate of flow i is

$$R_i^{fd} = \eta W \log_2\left(1 + \frac{P_r(t_i, r_i)}{N_0 W + \sum_\mu a_i^\mu P_r(t_j, r_i) + \sum_\mu b_i^\mu \beta_{t_i} P_t}\right), \tag{10}$$

where a_i^μ is a binary variable to denote whether flow i can receive the MUI from flow j. Thus, $\left(\sum_\mu a_i^\mu P_r(t_j, r_i)\right)$ is the total MUI received by flow i. b_i^μ represents if flow j has a common vertex with flow i. If so, $b_i^\mu = 1$; otherwise, $b_i^\mu = 0$. β_{t_i} is a constant which denotes the SI level at base station t_i. Accordingly, $\left(\sum_\mu b_i^\mu \beta_{t_i} P_t\right)$ is the SI received by flow i. Thus,

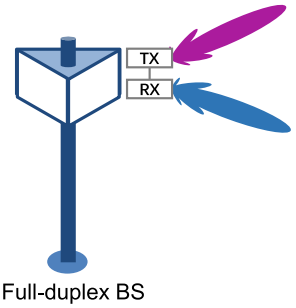

FIGURE 4. The full-duplex BS.

the throughput of flow i can be expressed as

$$Q_i^{fd} = \frac{R_i^{fd} \cdot \theta^{k_2}}{M}, \tag{11}$$

III. PROBLEM FORMULATION

In this paper, we focus on enhancing the energy efficiency of FD transmissions with given loads. As stated in [38], the total energy consumption of the proposed scheduling algorithm can be defined as

$$E = \sum_i \sum_{k_2} a_i^{k_2} P_t^i \cdot \theta^{k_2} \cdot \Delta T, \tag{12}$$

where $a_i^{k_2}$ is a binary variable and P_t^i is the scheduled transmission power of flow i. θ^{k_2} represents the number of CTAs allocated to group k_2, and ΔT is a constant denoting the time duration of one CTA. Therefore, to minimize E, we can consider minimizing $\sum_i \sum_{k_2} a_i^{k_2} P_t^i \cdot \theta^{k_2}$ under the following constraints.

First of all, a flow can only be scheduled in one specific group k_2, which can be denoted by

$$a_i^{k_2} = \begin{cases} 1, & flow\ i \in group\ k_2 \\ 0, & otherwise. \end{cases} \tag{13}$$

Secondly, with the capacity of one superframe fixed, the sum of CTAs allocated to each group should be less than or equal to M, which can be written as

$$\sum_{k_2} \theta^{k_2} \leq M. \tag{14}$$

Thirdly, considering the FD condition, conflicting flows, e.g., flow i and flow j, cannot be transmitted in the same group, as given in the following constraint

$$a_i^{k_2} + a_j^{k_2} \leq 1. \tag{15}$$

Then, to ensure the QoS in the concurrent transmission system, the throughput of each flow under the proposed algorithm should be larger than or at least equal to Q_i, which is achieved in the sequential TDMA mode. That can be written as

$$\frac{\sum_{k_2} R_i^{k_2} \cdot \theta^{k_2}}{M} \geq Q_i. \tag{16}$$

Finally, the transmission power of each flow after power control should satisfy

$$P_t^i \leq P_t. \tag{17}$$

In summary, to achieve the goal of energy efficiency that requires lower energy consumption with higher network throughput, the power consumption minimization problem of all flows based on concurrent transmission scheduling and power control can be modelled by

$$\min \sum_i \sum_{k_2} a_i^{k_2} P_t^i \cdot \theta^{k_2}$$
$$s.t. Constraints(11) - (15). \tag{18}$$

Like the problem proposed in [38], this is a Mixed Integer Nonlinear Programming (MINLP) problem. However, compared with the problem solved in [38], the FD mode, especially the system interference, is more complicated. Because the consideration of SI not only increases the difficulty in flow scheduling, but also enhances the complexity in power control. In the next section, we introduce an approach based on graph theory to simplify the problem and find a competitive solution.

IV. ENERGY EFFICIENT SCHEDULING Algorithm

In this section, the solution to Problem (18) is divided into three parts: construction of a contention graph, flow scheduling, and the power control algorithm. The flow scheduling based on contention graph enables concurrent transmission, which guarantees the network throughput. Then the transmission power of each flow is adjusted with throughput ensured, which decreases the energy consumption. Above all, it is found that as the transmission power of each flow decreases, the energy consumption reduces while the network throughput increases in return. Therefore, energy efficiency can be improved through the scheduling algorithm. Moreover, the overall complexity of the whole procedures is $\mathcal{O}(|V|^3)$.

A. CONTENTION GRAPH

According to graph theory, e.g., see [39], every flow can be denoted by a vertex and there is an edge between two vertices if severe interference exists between the two flows. Simultaneously, all concurrent transmission requirements and constraints under the FD mode can be modelled. Thus, as discussed in the end of Section II, concurrent transmission scheduling in a FD wireless backhaul network should consider not only the conflicts between data flows, but also the collisions caused by SI.

Firstly, according to the FD assumption, the two flows scheduled simultaneously either have no common node or one' s transmitter is the receiver of the other [13]. Thus, the three types of concurrent transmissions that are allowed in a FD network are illustrated in Fig. 5. Also note that the two concurrent transmission scenarios shown in Fig. 6 are not allowed since the two flows either have the same transmitting node or receiving node in these scenarios.

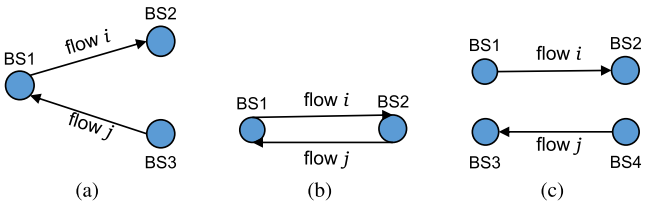

FIGURE 5. The cases of concurrent transmissions in a full-duplex network.

Secondly, to guarantee the data rate and throughput of each flow, the relative interference (RI) is defined to limit the concurrent transmission of flows. The reason is that when the RI between two flows is too large, the data rates of the flows become low [13], which is harmful to the system performance and QoS. However, the calculation of RI between flows varies under different allowed transmission scenarios. 1) For the case shown in Fig. 5(a), the RI received by flow j from flow i is RSI, which can be written as

$$RI_{ij} = \frac{N_0 W + \beta_{t_i} P_t}{P_t}, \tag{19}$$

whereas the RI received by flow i from flow j is MUI, which can be written as

$$RI_{ji} = \frac{N_0 W + P_r(t_j, r_i)}{P_t}. \tag{20}$$

2) For the case shown in Fig. 5(b), both the interference received by flow i from flow j and that received by flow j from flow i are RSI, which both can be calculated by (19). 3) For the case in Fig. 5(c), both the interference received by flow i from flow j and that received by flow j from flow i are MUI, which both can be calculated by (20).

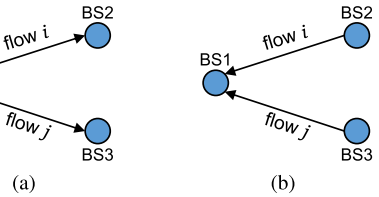

FIGURE 6. The cases that cannot transmit concurrently in the full-duplex system.

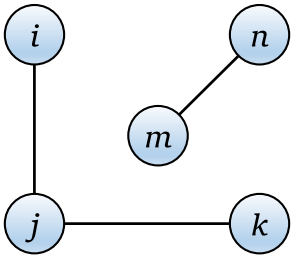

FIGURE 7. Contention graph.

Then if $\max\left(RI_{ij}, RI_{ji}\right) \geq \sigma$, we believe severe interference exists between flow i and flow j, so there is an edge between these two vertices in the contention graph, which means that these two flows cannot be transmitted concurrently. Here, σ is the interference threshold. Next, in Fig. 7, we show an example of contention graph based on this theory. As can be seen, flow i, flow j, and flow k are connected with edges, which means that there are conflicts among them, so that the concurrent transmission of flow i, flow j, and flow k is not allowed. The same holds for flow m and flow n.

B. FLOW SCHEDULING

According to the contention graph constructed, we can group all of the flows in the system. Inspired by [40], [41], the flows scheduled in one group can share allocated CTAs during their transmission, and the pseudocode of flow-grouping is shown in Algorithm 1.

Algorithm 1 Flow-Grouping Algorithm

Input : $Graph(V, E)$;
Output : Flow-Grouped results, $\mathbb{G}$;
Initialization: $\mathbb{G} \leftarrow \emptyset$;
1 **while** $V \neq \emptyset$ **do**
2 $G \leftarrow \emptyset$;
3 Obtain $v \in V$ with the minimum degree;
4 $G = G \cup v$;
5 $V = V - \{v\}$;
6 **foreach** v_i *in* V **do**
7 **foreach** v_j *in* G **do**
8 $e \leftarrow Edge\{v_i, v_j\}$;
9 **if** $e \notin E$ **then**
10 $G = G \cup \{v_i\}$;
11 $V = V - \{v_i\}$;
12 $\mathbb{G} = \mathbb{G} \cup \{G\}$;

Here, we denote the contention graph as $Graph(V, E)$, where V is the set of flows to be scheduled and E represents edges among flows. $\mathbb{G}$ is the flow-grouping results, in which the flows that can be transmitted concurrently are placed into the same subset. At the beginning of Algorithm 1, we initialize $\mathbb{G}$ as an empty set for the subsequent storage of grouped flows. Then in line 2, each group G is initialized as an empty set. Since in graph theory, the degree of each vertex represents the number of edges incident to it, we find out the vertex with the minimum degree and denote it as v in line 3, which is then scheduled into G. Line 6-11 try to find out the flows that can also be grouped into G iteratively, which do not have edges with v. When it comes to the procedure of iterative, we suppose there is an edge between v_i and v_j in line 8, and then determine whether this edge appears in the E of $Graph$. If not, v_i can be scheduled in group G and removed from V. It should be noted that V and G change dynamically in line 6-11 since once the conditional statement in line 9 is satisfied, the size of these two sets will be changed. The complexity of Algorithm 1 is $\mathcal{O}(|V|^2)$.

C. TRANSMISSION POWER CONTROL

Based on the flow-grouping results $\mathbb{G}$, we realize the decrease of energy consumption by adjusting the transmission power of each flow. This algorithm also accomplishes the actual throughput count after power control. The pseudocode is given in Algorithm 2, and the complexity is $\mathcal{O}(|V|)$.

In this algorithm, an empty set T is defined to save the number of CTAs in each group, whereas s is a variable initialized as 0 to sum each t. Line 2-7 express the procedure of CTAs allocation without power control in detail: Firstly, for every flow in one group, do the calculation of data rate with transmission power fixed as P_t using function $WithoutPC$, which can be denoted by (10). Next, the CTAs needed by each flow is determined by the formula in line 4. To guarantee the

Algorithm 2 Power Control & Throughput Count

Input : Flow-Grouped results, $\mathbb{G}$;
Required throughput of each flow Q_i;
Number of CTAs in a superframe, M;
Output : Power control result of each flow, P_t^i;
Actual throughput of each flow after power control, H_i;
Initialization: $T \leftarrow \emptyset, s = 0, P \leftarrow \emptyset, H \leftarrow \emptyset$;
1 **foreach** G *in* $\mathbb{G}$ **do**
2 **foreach** *flow* i *in* G **do**
3 $R_i^{fd1} = WithoutPC(P_t, \beta_{t_i})$;
4 $\xi_i = \lfloor Q_i \cdot M / R_i^{fd1} \rfloor$;
5 $t = max(\xi_i)$;
6 $T = T \cup \{t\}$;
7 $s = s + t$;
8 **foreach** G *in* $\mathbb{G}$ **do**
9 Obtain the corresponding t in T ;
10 **if** G *is not the last Group* **then**
11 $\theta = \lfloor M \cdot t / s \rfloor$;
12 **else**
13 θ is remaining unoccupied CTAs;
14 **foreach** *flow* i *in* G **do**
15 $R_i^{fd2} = Q_i \cdot M / \theta$;
16 $P_t^i = WithPC_1(R_i^{fd2}, \beta_{t_i}, P_t)$;
17 $P = P \cup \{P_t^i\}$;
18 **foreach** *flow* i *in* G **do**
19 $R_i^{fd3} = WithPC_2(P, \beta_{t_i})$;
20 $H_i = R_i^{fd3} \cdot M / \theta$;
21 $H = H \cup \{H_i\}$;
22 **return** P, *which is the set of* P_t^i,
23 H, *where actual throughput is stored*;

transmission of all flows in one group, the maximum value of ξ_i is assigned to t. Then t is stored in T and the value of s changes. These steps are performed iteratively until the CTAs required for each group is calculated.

In line 8-13, the CTAs of each group θ is re-allocated according to the proportion of t in s. To make full use of M time slots, when G is the last group, corresponding t is the remaining unallocated CTAs in this superframe. Next, the required data rate of each flow R_i^{fd2} with CTAs re-allocated is calculated in line 15. It is noted that the function $WithPC_1$ in line 16, which is given according to (10), can be expressed by

$$P_t^i = \frac{\left(2^{\frac{R_i^{fd2}}{\eta W}} - 1\right)\left(N_0 W + \sum_{\mu} a_i^{\mu} P_r(t_j, r_i) + \sum_{\mu} b_i^{\mu} \beta_{t_i} P_t\right)}{k G_t(t_i, r_i) G_r(t_i, r_i) D_{t_i r_i}^{-n}}, \quad (21)$$

where $\sum_{\mu} a_i^{\mu} P_r(t_j, r_i)$ and $\sum_{\mu} b_i^{\mu} \beta_{t_i} P_t$ represent the sum of MUI and SI received by flow i in the group G, respectively. Apparently, in each group, $\theta \geq t \geq \xi_i$ is satisfied for every flow, so that with the same Q_i guaranteed, R_i^{fd2}, the required data rate for flow i after power control is lower than, or equal to R_i^{fd1} in the worst situation. Thus, the transmission power of each flow $P_t^i \leq P_t$, and the whole energy consumed by the system will be lower.

Next, in line 18-21, we recalculate the actual throughput of each flow in Group G since after power control, the value of SI and MUI will be changed with the transmission power of all flows changed, which is illustrated in function $WithPC_2$ as

$$R_i^{fd3} = \eta W \log_2 \left(1 + \frac{P_r(t_i, r_i)}{N_0 W + \sum_{\mu} a_i^{\mu} P_r(t_j, r_i) + \sum_{\mu} b_i^{\mu} \beta_{t_i} P_t^i} \right). \tag{22}$$

It is noted that the transmission power in $P_r(t_i, r_i)$, $P_r(t_j, r_i)$, and $\sum_{\mu} b_i^{\mu} \beta_{t_i} P_t^i$ are all after power control. Finally, P and H, which store the adjusted transmission powers and actual throughput, are returned back.

V. SIMULATION AND ANALYSIS

A. SIMULATION SETUP

The simulation is proposed in a 60 GHz mmWave wireless backhaul network and the realistic directional antennas explained in (1) are adopted. With the assumption of LOS transmission, the path loss exponent is 2 [42]. According to [37], the typical FD systems provide SI cancellation of approximately 120 dB. Thus, the SI cancellation factor used in the simulation is uniformly distributed in $2 \times 10^{11.5}$ to $4 \times 10^{11.5}$. At the beginning, 10 BSs supporting FD transmission are stochastically distributed in the range of $100 \times 100\ m^2$ and every BS has the same transmission power P_t. As each flow selects transceivers randomly, the transmission distance is also uncertain. Simulations are implemented in MATLAB and the detailed initial parameters are listed in Table 1.

We evaluate the performance of the proposed FD concurrent scheduling algorithm (Proposed-FD) and compare it with three existing schemes, i.e., TDMA, HD concurrent transmission scheme with power control (Proposed-HD), and FD concurrent transmission scheme without power control (CTFP).

To clarify performance comparison, we propose two traffic load models. In traffic A, the number of flows are fixed as 10, where the required throughput of each flow changes among [0.5 , 1.5] Gbps, [1 , 2] Gbps, [1.5 , 2.5] Gbps, [2 , 2.5] Gbps and [2.5 , 3.5] Gbps, which are denoted by the traffic load from 1 to 5, respectively. In traffic B, the number of flows ranges from 6 to 10, which is denoted by the x-axis in Fig. 8 (b), Fig. 9 (b), and Fig. 10 (b), whereas the required throughput of each flow is uniformly distributed in [2.5 , 3.5] Gbps.

TABLE 1. Initial parameters.

Parameter	Symbol	Value
Number of CTAs	M	5000
Background noise	N_0	-134 dBm/MHz
System bandwidth	W	2100 MHz
Maximum transmission power	P_t	40 dBm
Transceiver efficiency	η	0.5
Path loss exponent	n	2
MUI factor	ρ	0.007
One CTA duration	ΔT	18 μs
Half-power beamwidth	θ_{-3dB}	30°
Threshold	σ	10^{-10}

B. PERFORMANCE EVALUATION OF THE PROPOSED ALGORITHM

To fully demonstrate the superiority of Proposed-FD, performance evaluation is performed in the following dimensions such as energy consumption, network throughput, and energy efficiency. The value of the interference threshold is fixed as 10^{-10}, whereas the simulation results are an average of 50 times experiments.

1) REDUCED ENERGY CONSUMPTION

In Fig. 8(a), under Traffic A, the energy consumption of four schemes including TDMA, Proposed-HD, Proposed-FD, and CTFP is plotted in the unit of Joule (J). As we can see, compared with the serial transmission, concurrent transmission with power control consumes lower energy, in which Proposed-FD outperforms Proposed-HD, especially under heavy traffic loads. This is because the FD mode allows more flows to be transmitted simultaneously, which further reduces energy consumption. At traffic load 5, Proposed-FD saves about 55.6%, 84.2%, and 43.1% energy compared with TDMA, CTFP, and Proposed-HD, respectively. In CTFP, although concurrent transmission is deployed, the transmission power of each flow is fixed as the maximum P_t with all CTAs occupied, which does not lead to energy saving. It is also the reason why CTFP is not sensitive to traffic load growth while the energy consumption of the other three mechanism increases with heavier traffic load deployed.

In Fig. 8(b), we plot the energy consumption of these four schemes under Traffic B. As can be seen, with the number of flows increases, the energy consumed by each mechanism is increasing. The Proposed-FD still costs the lowest power whereas the energy consumed by the CTFP remains high. In summary, the Proposed-FD algorithm consumes the least energy among these four schemes, which is clearer at high traffic load or with more flows scheduled.

2) ENHANCED NETWORK THROUGHPUT

In Fig. 9(a), the network throughput of these four schemes under Traffic A is displayed in the unit of Gbps. It can be seen that the throughput achieved by our Proposed-FD algorithm

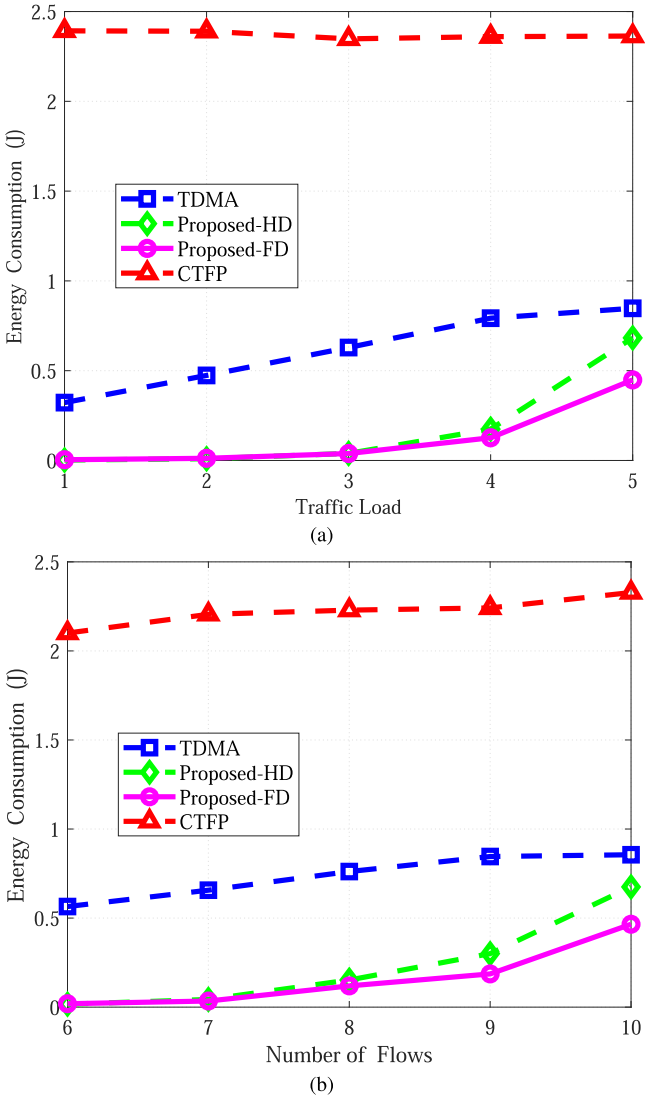

FIGURE 8. The comparison of energy consumption(J). (a) under Traffic A. (b) under Traffic B.

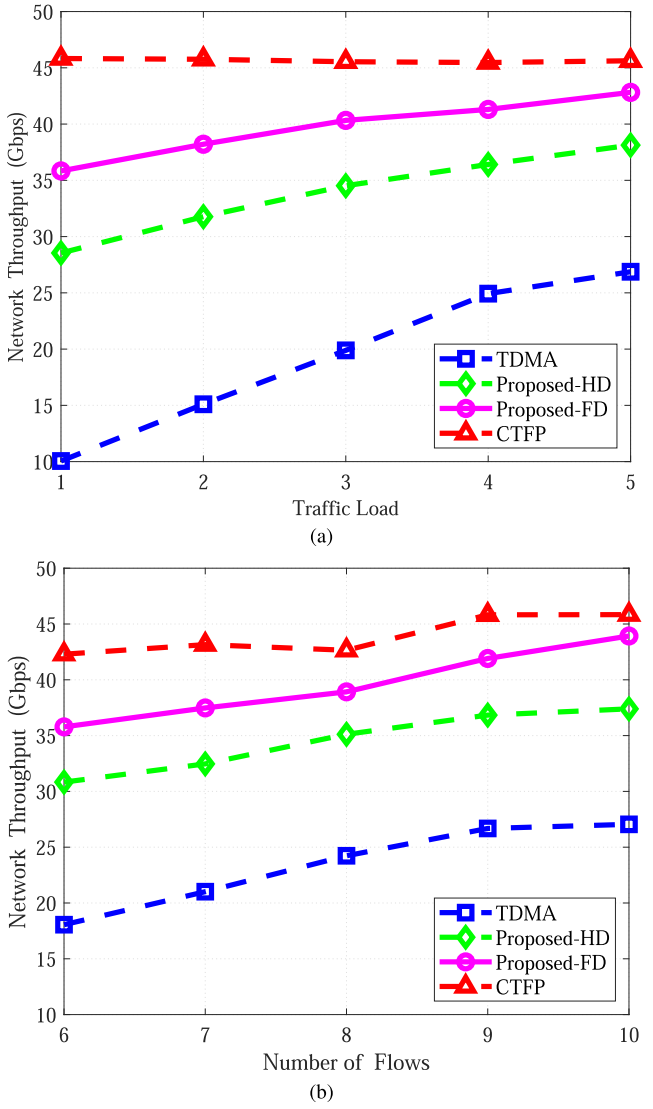

FIGURE 9. The comparison of network throughput(Gbps). (a) under Traffic A. (b) under Traffic B.

is inferior to CTFP, but significantly exceeds TDMA and Proposed-HD. Just as described in (22), the actual data rate of each flow becomes larger after power control since each scheduled transmission power will be lower than P_t, which leads to the increase of actual throughput. The algorithm of this part is listed in line 18-21 of Algorithm.2. The fact is that as traffic load increases, the gap between Proposed-FD and TDMA decreases, because under light loads, the transmission power can be further reduced by allocating more CTAs to each group in Proposed-FD. It is noted that the throughput of Proposed-HD and Proposed-FD grows almost at the same rate. The reason is that these two schemes both adopt parallel transmission principle. The difference is that the FD algorithm gives a further improvement for its parallel transmission. Finally, when the traffic load changes, the throughput of CTFP is always relatively steady because with the maximum transmission power P_t and all CTAs used, the growth of traffic load does not have an impact on its energy consumption or throughput.

In Fig. 9(b), we plot the network throughput of these four schemes under Traffic B. As we can observe, except for CTFP, the throughput grows with the increase of flow number. Especially for the Proposed-FD, when the flow number is large, its throughput is very close to that of CTFP. For example, when the flow number is 10, the throughput of Proposed-FD is only about 4.2% lower than that of CTFP, but twice of TDMA and 1.2 times of Proposed-HD, which benefits from concurrent transmission and SI cancellation. In summary, the Proposed-FD algorithm achieves network throughput enhancement compared to TDMA and Proposed-HD. Attention should be paid to the fact that CTFP achieves the highest throughput with high energy costs, whose energy efficiency is actually lower than the Proposed-FD algorithm.

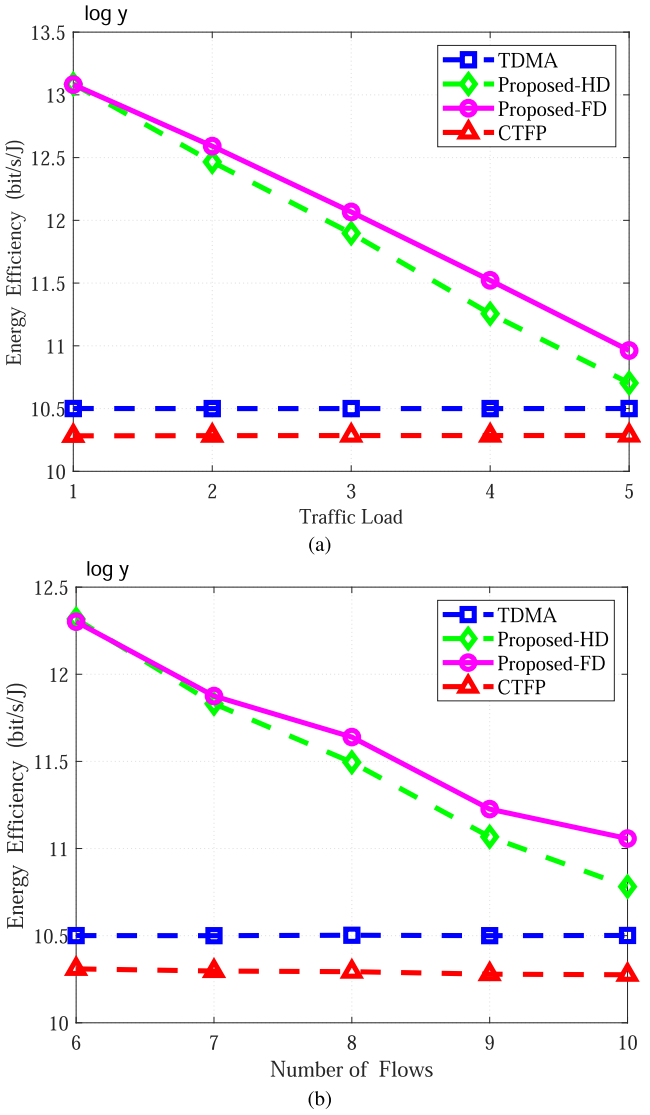

FIGURE 10. The comparison of energy efficiency. (a) under Traffic A. (b) under Traffic B.

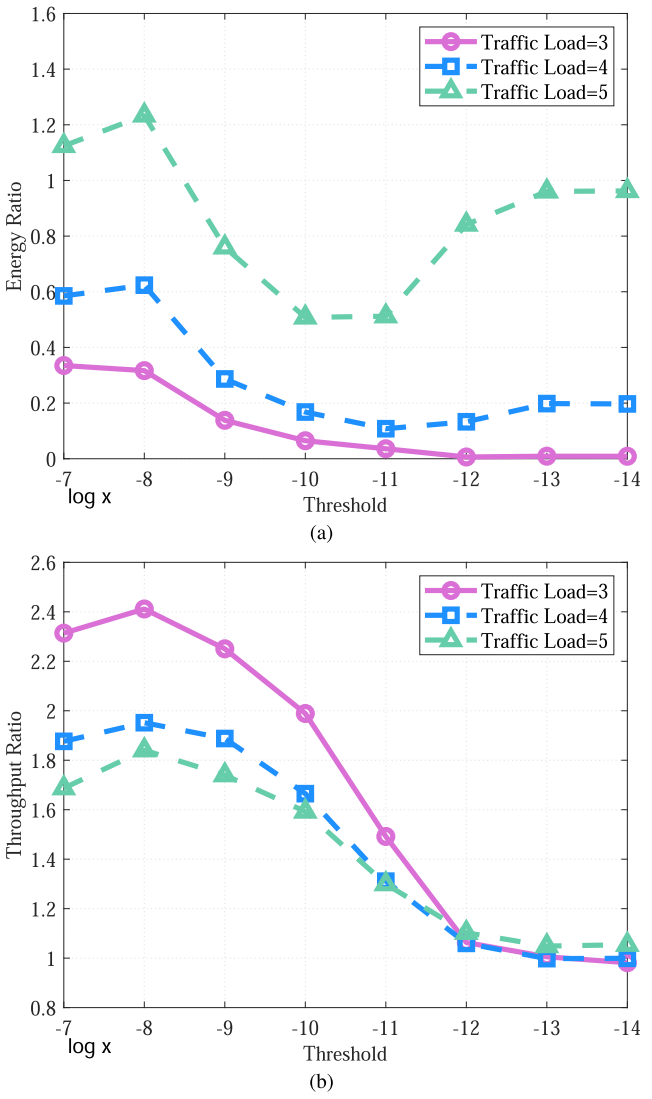

FIGURE 11. Energy Ratio and Throughput Ratio under different Traffic Load. (a) Energy Ratio. (b) Throughput Ratio.

3) HIGHER ENERGY EFFICIENCY

Dividing the throughput in Fig. 9(a) by the energy consumption in Fig. 8(a), the energy efficiency of these four schemes under Traffic A is plotted in Fig. 10(a), where the unit is bit/s/J and the y-axis value is taken after $\log_{10}$. It can be observed that our Proposed-FD achieves the best energy efficiency, which decreases with the growth of load, because transmission power will be larger under heavy load, leading to increased interference and decreased efficiency. Similarly, the Proposed-HD is superior to TDMA and CTFP, which also benefits from the concurrent transmission and power control. TDMA is more energy efficient than CTFP since the latter consumes much more power, which offsets the advantages of parallel transmission.

In Fig. 10(b), the energy efficiency of these four schemes under Traffic B is plotted. As the flow number increases, the trend of these four schemes is basically the same as that of Fig. 10(a). It is noted that the gap between Proposed-HD and Proposed-FD becomes larger with flow number increasing, indicating that Proposed-FD is more suitable to be deployed in high traffic communication. In a word, Proposed-FD always shows better performance in energy efficiency.

C. THE CHOICE OF THRESHOLD

Inspired by [38], we analyze the influence on Proposed-FD under different interference thresholds σ. Energy Ratio is defined as the energy consumption of our scheme divided by that of TDMA, while throughput ratio is denoted by the throughput achieved in our scheme divided by that of TDMA. In this part, traffic model A is adopted and the x-axis of each figure is the value of $\log_{10}\sigma$.

1) UNDER VARIABLE TRAFFIC LOADS

In Fig. 11(a), we can observe that the line under traffic load 5 and 4 first decreases and then increases, which achieves its minimum value 0.58 at $x = -10$ and 0.12 at $x = -11$,

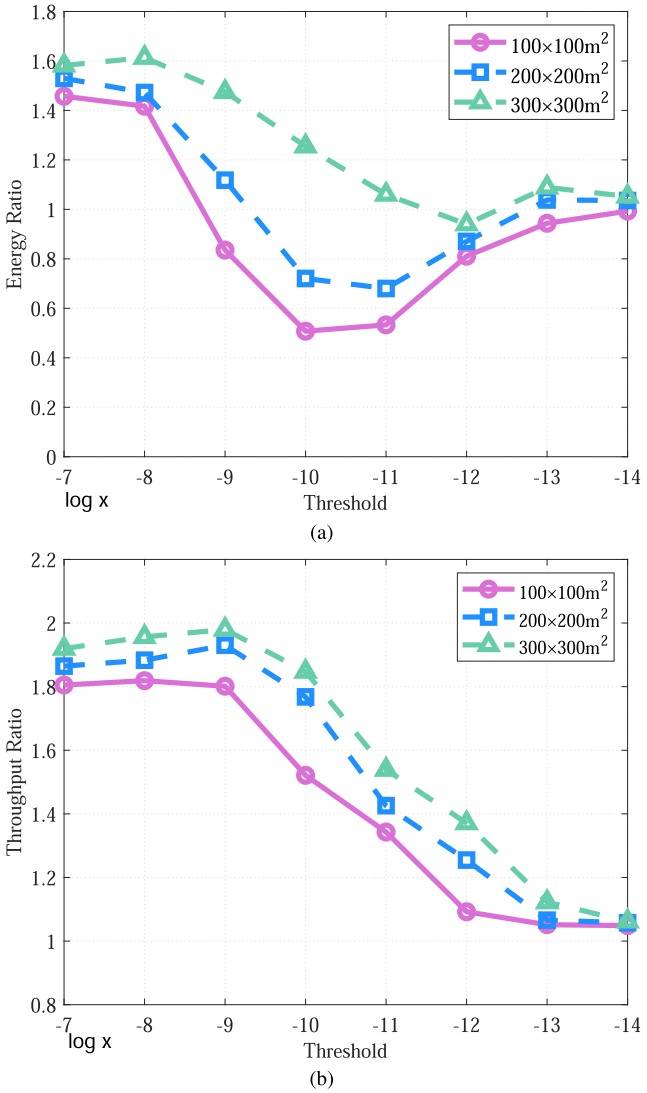

FIGURE 12. Energy Ratio and Throughput Ratio under different BS distribution. (a) Energy Ratio. (b) Throughput Ratio.

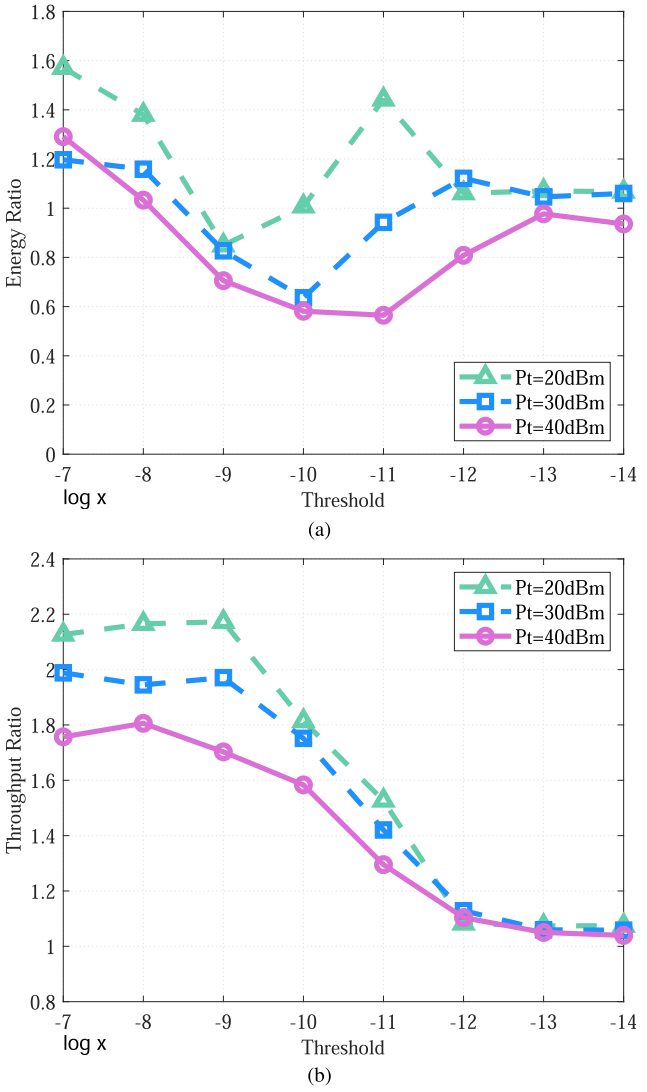

FIGURE 13. Energy Ratio and Throughput Ratio under different maximum transmission power. (a) Energy Ratio. (b) Throughput Ratio.

respectively, which means that the most suitable threshold differs under variable loads. When traffic load is heavy, the threshold should be smaller to save energy. By vertical observation, to meet the increasing required throughput, the transmission power of each flow should be larger, which will cause severe interference between concurrent transmission flows and ultimately cause higher energy consumption.

The throughput ratio under different traffic loads is plotted in Fig. 11(b). Under light load, the superiority of our algorithm is more obvious, which declines slowly and close to 1 when the threshold is smaller than 10^{-11}. The fact is that more CTAs can be allocated to each group under light load, which is beneficial to realize lower energy consumption and higher network throughput than TDMA.

2) UNDER VARIABLE BS DISTRIBUTIONS

In this part, we assume that there are 10 flows under traffic load 5 in the simulation. In Fig. 12(a), we plot the energy ratio of Proposed-FD over TDMA when the 10 BSs are uniformly distributed in $100 \times 100\ m^2$, $200 \times 200\ m^2$, and $300 \times 300\ m^2$ area, respectively. As can be seen, the lowest energy ratio is realized when the threshold is 10^{-10} with BSs distributed in the $100 \times 100\ m^2$ area, whereas this point is achieved at the threshold of 10^{-11} in the $200 \times 200\ m^2$ area and 10^{-12} in the $300 \times 300\ m^2$ area. It is illustrated that with BSs distributed densely, the energy ratio becomes lower, and the threshold can be larger. This is because in mmWave networks, transmission power attenuates strongly as the propagation distance increases, so that if the same throughput is to be satisfied in a wider area, more energy will be consumed. As we expected, when the threshold becomes very small, the concurrent transmission reduces to TDMA, so that the energy ratio is close to 1.

We compare the throughput ratio when the BS distribution differs in Fig. 12(b). It is clear that the best performance

appears at the threshold of 10^{-9} when the BSs are distributed in the $200 \times 200\ m^2$ or $300 \times 300\ m^2$ area, whereas that in the $100 \times 100\ m^2$ area should be 10^{-8}. This feature should be taken into account when the threshold is determined. Then, the throughput ratio in $300 \times 300\ m^2$ shows superiority to the others, because larger transmission power should be used when the transmission distance increases, and the sparse BSs distribution helps to reduce the MUI, which together improve the transmission data rate and enhance the network throughput.

3) UNDER VARIABLE MAXIMUM TRANSMISSION POWER P_t

In this part, there are 10 flows whose required throughput is uniformly distributed in [2.5 , 3.5] Gbps. In Fig. 13(a), we plot the energy ratio of Proposed-FD over TDMA with P_t fixed as 20 dBm, 30 dBm, 40 dBm, respectively. It is found that the energy ratio reaches different minimum values as P_t differs. Further, as the transmission power grows, the threshold should be smaller to degrade concurrent transmission interference.

The throughput ratio under variable P_t is also compared in Fig. 13(b), which all grow at first and then decrease, and finally approach to 1. The point is that, when the threshold is larger than 10^{-12}, the smaller P_t we choose, the larger throughput ratio can be achieved. In summary, to achieve low energy ratio and high throughput ratio, the selection of threshold should consider the transmission power.

In this section, the choice of interference thresholds takes the traffic loads, BS distributions, and maximum transmission powers into consideration, which should also pay attention to the balance of energy ratio and throughput ratio.

VI. CONCLUSION

In this paper, to take advantage of advanced SI cancellation techniques, we proposed a FD concurrent transmission algorithm based on a contention graph for the mmWave backhaul network. The construction of contention graph provided a novel method for flow-grouping transmission scheduling, and the proposed power control algorithm achieved energy saving and throughput enhancement. Simulation results clearly showed that the energy efficiency of Proposed-FD was superior to existing TDMA, CTFP, and Proposed-HD schemes. Extensive numerical studies also found that the choice of interference thresholds was related to traffic loads, BS distributions, and maximum transmission powers, which greatly influenced the system performance.

In a mmWave wireless backhaul system, except for transmission power and modes, circuit power and interface power should also be considered in the power consumption model. In this paper, we only research the energy efficiency of a mmWave backhaul network under different transmission power and modes. To find further optimization solution, we will jointly optimize the power consumption of the system in the future.

REFERENCES

[1] S. Hur, T. Kim, D. J. Love, J. V. Krogmeier, T. A. Thomas, and A. Ghosh, "Millimeter wave beamforming for wireless backhaul and access in small cell networks," *IEEE Trans. Commun.*, vol. 61, no. 10, pp. 4391–4403, Oct. 2013.

[2] Z. Tan, H. Qu, J. Zhao, G. Ren, and W. Wang, "Low-complexity networking based on joint energy efficiency in ultradense mmWave backhaul networks," *Trans. Emerg. Telecommun. Technol.*, vol. 30, no. 1, 2019, Art. no. e3508. [Online]. Available: https://onlinelibrary.wiley.com/doi/abs/10.1002/ett.3508

[3] H. S. Dhillon and G. Caire, "Wireless backhaul networks: Capacity bound, scalability analysis and design guidelines," *IEEE Trans. Wireless Commun.*, vol. 14, no. 11, pp. 6043–6056, Nov. 2015.

[4] Z. Xiao, L. Zhu, J. Choi, P. Xia, and X.-G. Xia, "Joint power allocation and beamforming for non-orthogonal multiple access (NOMA) in 5G millimeter wave communications," *IEEE Trans. Wireless Commun.*, vol. 17, no. 5, pp. 2961–2974, May 2018.

[5] X. Ge, H. Cheng, M. Guizani, and T. Han, "5G wireless backhaul networks: Challenges and research advances," *IEEE Netw.*, vol. 28, no. 6, pp. 6–11, Nov. 2014.

[6] K. R. Malekshan, W. Zhuang, and Y. Lostanlen, "An energy efficient MAC protocol for fully connected wireless ad hoc networks," *IEEE Trans. Wireless Commun.*, vol. 13, no. 10, pp. 5729–5740, Oct. 2014.

[7] G. Hosseinabadi and N. Vaidya, "Concurrent-MAC: Increasing concurrent transmissions in dense wireless LANs," in *Proc. IEEE ICNC*, Kauai, HI, USA, Feb. 2016, pp. 1–5.

[8] H. Hasegawa and H. Kanai, "High-frame-rate echocardiography using diverging transmit beams and parallel receive beamforming," *J. Med. Ultrason.*, vol. 38, no. 3, pp. 129–140, Jul. 2011, doi: 10.1007/s10396-011-0304-0.

[9] M. Veyseh, A. Anpalagan, and B. Ma, "Adaptive channel and superframe allocation (ACSA) for 60 GHz wireless networks," *Math. Comput. Model.*, vol. 53, no. 3, pp. 405–420, Feb. 2011. [Online]. Available: http://www.sciencedirect.com/science/article/pii/S0895717710001457

[10] E. Toscano and L. L. Bello, "Multichannel superframe scheduling for IEEE 802.15.4 industrial wireless sensor networks," *IEEE Trans. Ind. Informat.*, vol. 8, no. 2, pp. 337–350, May 2012.

[11] P. Xu and H. Chu, "A novel link scheduling strategy for concurrent transmission in mmWave WPANs based on beamforming information," in *Proc. IEEE WCNC*, Istanbul, Turkey, Apr. 2014, pp. 1709–1714.

[12] Z. Zhang, X. Chai, K. Long, A. V. Vasilakos, and L. Hanzo, "Full duplex techniques for 5G networks: Self-interference cancellation, protocol design, and relay selection," *IEEE Commun. Mag.*, vol. 53, no. 5, pp. 128–137, May 2015.

[13] W. Ding, Y. Niu, H. Wu, Y. Li, and Z. Zhong, "QoS-aware full-duplex concurrent scheduling for millimeter wave wireless backhaul networks," *IEEE Access*, vol. 6, pp. 25313–25322, 2018.

[14] A. Nadh, S. Joseph, A. Sharma, S. Aniruddhan, and R. K. Ganti, "A linearization technique for self-interference cancellation in full-duplex radios," *CoRR*, pp. 1–11, May 2016. [Online]. Available: http://arxiv.org/abs/1605.01345

[15] A. Sahai, G. Patel, and A. Sabharwal, "Pushing the limits of full-duplex: Design and real-time implementation," *CoRR*, pp. 1–12, Jul. 2011. [Online]. Available: http://arxiv.org/abs/1107.0607

[16] B. Kaufman, J. Lilleberg, and B. Aazhang, "An analog baseband approach for designing full-duplex radios," in *Proc. Asilomar Conf. Signals, Syst. Comput.*, Pacific Grove, CA, USA, Nov. 2013, pp. 987–991.

[17] L. Wang, S. Liu, M. Chen, G. Gui, and H. Sari, "Sidelobe interference reduced scheduling algorithm for mmWave device-to-device communication networks," *Peer-to-Peer Netw. Appl.*, vol. 12, no. 1, pp. 228–240, Jan. 2019, doi: 10.1007/s12083-018-0660-2.

[18] J. Deng, O. Tirkkonen, R. Freij-Hollanti, T. Chen, and N. Nikaein, "Resource allocation and interference management for opportunistic relaying in integrated mmWave/sub-6 GHz 5G networks," *IEEE Commun. Mag.*, vol. 55, no. 6, pp. 94–101, Jun. 2017.

[19] Z. Xiao, P. Xia, and X.-G. Xia, "Enabling UAV cellular with millimeter-wave communication: Potentials and approaches," *IEEE Commun. Mag.*, vol. 54, no. 5, pp. 66–73, May 2016.

[20] S. Noh, M. D. Zoltowski, and D. J. Love, "Multi-resolution codebook and adaptive beamforming sequence design for millimeter wave beam alignment," *IEEE Trans. Wireless Commun.*, vol. 16, no. 9, pp. 5689–5701, Sep. 2017.

[21] Z. Xiao, T. He, P. Xia, and X.-G. Xia, "Hierarchical codebook design for beamforming training in millimeter-wave communication," *IEEE Trans. Wireless Commun.*, vol. 15, no. 5, pp. 3380–3392, May 2016.
[22] H. He, C.-K. Wen, S. Jin, and G. Y. Li, "Deep learning-based channel estimation for beamspace mmWave massive MIMO systems," *IEEE Wireless Commun. Lett.*, vol. 7, no. 5, pp. 852–855, Oct. 2018.
[23] A. M. Hamed and R. K. Rao, "Evaluation of capacity and power efficiency in millimeter-wave bands," in *Proc. IEEE SPECTS*, Montreal, QC, Canada, Jul. 2016, pp. 1–6.
[24] Z. Xiao, C. Zhang, D. Jin, and N. Ge, "GLRT approach for robust burst packet acquisition in wireless communications," *IEEE Trans. Wireless Commun.*, vol. 12, no. 3, pp. 1127–1137, Mar. 2013.
[25] L. Zhu, J. Zhang, Z. Xiao, X. Cao, D. O. Wu, and X.-G. Xia, "Millimeter-wave NOMA with user grouping, power allocation and hybrid beamforming," *IEEE Trans. Wireless Commun.*, vol. 18, no. 11, pp. 5065–5079, Nov. 2019.
[26] Z. Xiao, X. G. Xia, and L. Bai, "Achieving antenna and multipath diversities in GLRT-based burst packet detection," *IEEE Trans. Signal Process.*, vol. 63, no. 7, pp. 1832–1845, Apr. 2015.
[27] Y. Li, Y. Dong, X. Zhang, J. Jiang, and Z. Shao, "A wideband directional mm-wave antenna for micro-deformation monitoring radar applications," in *Proc. IEEE Int. Symp. Antennas Propag. USNC/URSI Nat. Radio Sci. Meeting*, Boston, MA, USA, Jul. 2018, pp. 1307–1308.
[28] I. K. Son, S. Mao, M. X. Gong, and Y. Li, "On frame-based scheduling for directional mmWave WPANs," in *Proc. IEEE INFOCOM*, Orlando, FL, USA, Mar. 2012, pp. 2149–2157.
[29] I. K. Son, S. Mao, Y. Li, M. Chen, M. X. Gong, and T. S. Rappaport, "Frame-based medium access control for 5G wireless networks," *Mobile Netw. Appl.*, vol. 20, no. 6, pp. 763–772, Dec. 2015.
[30] Z. Guo, R. Yao, W. Zhu, X. Wang, and Y. Ren, "Intra-superframe power management for IEEE 802.15.3 WPAN," *IEEE Commun. Lett.*, vol. 9, no. 3, pp. 228–230, Mar. 2005.
[31] C. Qian, X. Peng, J. Yang, and F. Chin, "Spatial reuse strategy in mmWave WPANs with directional antennas," in *Proc. IEEE GLOBECOM*, Anaheim, CA, USA, Dec. 2012, pp. 5392–5397.
[32] L. X. Cai, L. Cai, X. Shen, and J. W. Mark, "REX: A randomized exclusive region based scheduling scheme for mmWave WPANs with directional antenna," *IEEE Trans. Wireless Commun.*, vol. 9, no. 1, pp. 113–121, Jan. 2010.
[33] J. Qiao, L. X. Cai, X. Shen, and J. W. Mark, "STDMA-based scheduling algorithm for concurrent transmissions in directional millimeter wave networks," in *Proc. IEEE ICC*, Ottawa, ON, Canada, Jun. 2012, pp. 5221–5225.
[34] S. H. Chae and K. Lee, "Degrees of freedom of full-duplex cellular networks: Effect of self-interference," *IEEE Trans. Commun.*, vol. 65, no. 10, pp. 4507–4518, Oct. 2017.
[35] E. Ahmed and A. M. Eltawil, "All-digital self-interference cancellation technique for full-duplex systems," *IEEE Trans. Wireless Commun.*, vol. 14, no. 7, pp. 3519–3532, Jul. 2015.
[36] E. Everett, A. Sahai, and A. Sabharwal, "Passive self-interference suppression for full-duplex infrastructure nodes," *IEEE Trans. Wireless Commun.*, vol. 13, no. 2, pp. 680–694, Jan. 2014.
[37] M. S. Sim, M. Chung, D. Kim, J. Chung, D. K. Kim, and C.-B. Chae, "Nonlinear self-interference cancellation for full-duplex radios: From link-level and system-level performance perspectives," *IEEE Commun. Mag.*, vol. 55, no. 9, pp. 158–167, Jun. 2017.
[38] Y. Niu, C. Gao, Y. Li, L. Su, D. Jin, Y. Zhu, and D. O. Wu, "Energy-efficient scheduling for mmWave backhauling of small cells in heterogeneous cellular networks," *IEEE Trans. Veh. Technol.*, vol. 66, no. 3, pp. 2674–2687, Mar. 2017.
[39] T. D. Hoang, L. B. Le, and T. Le-Ngoc, "Resource allocation for D2D communication underlaid cellular networks using graph-based approach," *IEEE Trans. Wireless Commun.*, vol. 15, no. 10, pp. 7099–7113, Oct. 2016.
[40] M. X. Gong, D. Akhmetov, R. Want, and S. Mao, "Directional CSMA/CA protocol with spatial reuse for mmWave wireless networks," in *Proc. IEEE GLOBECOM*, Miami, FL, USA, Dec. 2010, pp. 1–5.
[41] Z. He, S. Mao, S. Kompella, and A. Swami, "Link scheduling and channel assignment with a graph spectral clustering approach," in *Proc. IEEE MILCOM*, Baltimore, MD, USA, Nov. 2016, pp. 73–78.
[42] S. Geng, J. Kivinen, X. Zhao, and P. Vainikainen, "Millimeter-wave propagation channel characterization for short-range wireless communications," *IEEE Trans. Veh. Technol.*, vol. 58, no. 1, pp. 3–13, Jan. 2009.

JING LI received the B.E. degree from Beijing Information Science and Technology University, China, in 2016. She is currently pursuing the M.S. degree with Beijing Jiaotong University. Her research interests include millimeter wave communications and medium access control.

YONG NIU (S'13–M'16) received the B.E. degree in electrical engineering from Beijing Jiaotong University, China, in 2011, and the Ph.D. degree in electronic engineering from Tsinghua University, Beijing, China, in 2016.

From November 2014 to April 2015, he visited the University of Florida, Gainesville, FL, USA, as a Visiting Scholar. He is currently an Associate Professor with the State Key Laboratory of Rail Traffic Control and Safety, Beijing Jiaotong University. His research interests are in the areas of networking and communications, including millimeter wave communications, device-to-device communication, medium access control, and software-defined networks. He received the Ph.D. National Scholarship of China in 2015, Outstanding Ph.D. Graduates and Outstanding Doctoral thesis of Tsinghua University, in 2016, and Outstanding Ph.D. Graduates of Beijing, in 2016. He has served as the Technical Program Committee (TPC) member for CHINACOM 2015 and IWCMC 2017, and also the session chair for IWCMC 2017 and CHINACOM 2017.

HAO WU (M'10) received the Ph.D. degree in information and communication engineering from the Harbin Institute of Technology, in 2000. She is currently a Full Professor with the State Key Laboratory of Rail Traffic Control and Safety at Beijing Jiaotong University (BJTU), China. She has published more than 100 international journal articles and conference papers. Her research interests include intelligent transportation systems (ITS), security and QoS issues in wireless networks (VANETs, MANETs, and WSNs), wireless communications, and the Internet of Things (IoT). She is a Reviewer of its major conferences and journals in wireless networks and security.

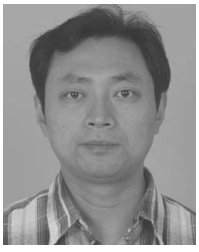

BO AI (M'00–SM'10) received the M.S. and Ph.D. degrees from Xidian University, China, in 2002 and 2004, respectively.

He is currently a Full Professor and the Ph.D. Student Advisor with the State Key Laboratory of Rail Traffic Control and Safety, Beijing Jiaotong University, China. He is the Deputy Director of the State Key Laboratory of Rail Traffic Control and Safety. He has authored/coauthored six books and published over 230 academic research articles. He holds 21 invention patents. He is a fellow of the Institution of Engineering and Technology. He is also an Associate Editor of the IEEE TRANSACTIONS ON CONSUMER ELECTRONICS and an editorial committee member of wireless personal communications.

ZHANGDUI ZHONG (M'15–SM'17) received the B.S. and M.S. degrees from Beijing Jiaotong University (BJTU), China, in 1983 and 1988, respectively.

He is currently a Professor with BJTU and a Chief Scientist with the State Key Laboratory of Rail Traffic Control and Safety, BJTU and the Ministry of Railways, China. He is also a Director of the Innovative Research Team of the Ministry of Education. His research interests include wireless communications for railways, control theory and techniques for railways, and global system for mobile communications-railway. He received the Mao Yisheng Scientific Award of China, the Zhan Tianyou Railway Honorary Award of China, and the Top Ten Science/Technology Achievements Award of Chinese Universities.

SHIWEN MAO (S'99–M'04–SM'09–F'19) received the Ph.D. degree in electrical and computer engineering from Polytechnic University (now The New York University Tandon School of Engineering), Brooklyn, NY, USA.

He was the McWane Associate Professor from 2012 to 2015. He is currently the Samuel Ginn Distinguished Professor with the Department of Electrical and Computer Engineering, and the Director of the Wireless Engineering Research and Education Center, Auburn University, Auburn, AL, USA. His research interests include wireless networks, multimedia communications, and smart grid.

He received the IEEE ComSoc TC-CSR Distinguished Technical Achievement Award, in 2019, the IEEE ComSoc MMTC Distinguished Service Award, in 2019, Auburn University Creative Research and Scholarship Award, in 2018, the 2017 IEEE ComSoc ITC Outstanding Service Award, the 2015 IEEE ComSoc TC-CSR Distinguished Service Award, and the 2013 IEEE ComSoc MMTC Outstanding Leadership Award, and NSF CAREER Award in 2010. He is a co-recipient of the IEEE ComSoc MMTC Best Journal Paper Award, in 2019, the IEEE ComSoc MMTC Best Conference Paper Award, in 2018, the Best Demo Award from the IEEE SECON 2017, the Best Paper Awards, from the IEEE GLOBECOM 2019, 2016, and 2015, the IEEE WCNC 2015, and the IEEE ICC 2013, and the 2004 IEEE Communications Society Leonard G. Abraham Prize in the field of communications systems. He was a Distinguished Lecturer, from 2014 to 2018 of the IEEE Vehicular Technology Society and a Distinguished Speaker, from 2018 to 2021. He is an Area Editor of the IEEE TRANSACTIONS ON WIRELESS COMMUNICATIONS, the IEEE OPEN JOURNAL OF THE COMMUNICATIONS SOCIETY, the IEEE INTERNET OF THINGS JOURNAL, the IEEE/CIC China Communications, and ACM GetMobile, and an Associate Editor of the IEEE TRANSACTIONS ON NETWORK SCIENCE AND ENGINEERING, the IEEE TRANSACTIONS ON MULTIMEDIA, the IEEE TRANSACTIONS ON MOBILE COMPUTING, the IEEE MULTIMEDIA, and the IEEE NETWORKING LETTERS, among others.